ACS OMEGA

http://pubs.acs.org/journal/acsodf

Article

Mantle-Derived Helium Distribution and Tectonic Implications in the Sichuan−Yunnan Block, China

Bingkun Meng, Shixin Zhou,* Jing Li,* and Zexiang Sun

Cite This: *ACS Omega* 2021, 6, 30674−30685

Read Online

ACCESS | Metrics & More | Article Recommendations

ABSTRACT: The geochemical characteristics of mantle degassing observed on the surface of the earth can indicate the origin and migration path of mantle fluids. Compared with the plate boundary tectonic environment, the intraplate tectonic environment does not have a large number of active volcanoes and active faults, and the observation of mantle volatiles in hot spring gas is relatively limited. We selected the Sichuan−Yunnan block to discuss mantle degassing based on the carbon and noble gas isotopes of the spring gases and previous studies on the fault slip rate and geophysical research. A total of five hot spring gas samples (including two free gases and three dissolved gases) were collected from the Sichuan−Yunnan block. Chemical and isotopic compositions were analyzed in N_2-dominant hot spring gases. The $^3He/^4He$ ratio (0.068−0.541 R_a) indicates the occurrence of mantle-derived helium throughout the Sichuan−Yunnan block, which has been diluted by a crustal radiogenic ^4He component. The occurrence of mantle-derived helium in the study areas ranges from 0.74 to 5.67%. The lower proportion of mantle-derived helium in YNWQ and HGWQ than that in other spring gases near the Jinghe-Qinghe fault may be caused by the smaller scale of fault around YNWQ and HGWQ than the Jinghe-Qinghe fault. The correlation between ^4He, ^{20}Ne, and N_2 concentrations implies a common trapping mechanism for ^4He, ^{20}Ne, and N_2 in hot spring gases. The $^{40}Ar/^{36}Ar$ ratios and N_2/Ar ratios indicate that N_2 and Ar are mostly meteoric, and YNWQ and HGWQ have more crustal-derived Ar contribution (40.56 and 51.49%, respectively). The $\delta^{13}C(CO_2)_o$ values calculated by Rayleigh fractionation and CO_2 concentration suggest that CO_2 has inorganic and organic origins. The plot of R_c/R_a versus $\delta^{13}C(CO_2)$ indicates that the spring gas CO_2 origin in the Sichuan−Yunnan block is mainly derived from mixing of limestone and organic sediments with minor mantle CO_2. The $\delta^{13}C(CH_4)$ versus $CH_4/^3He$ values indicate that the origin of methane is thermogenic and microbial oxidation. The low mantle-derived helium distribution pattern is most likely controlled by the weak fault activity rate, the small fault scale, and not obvious magmatic activity in the Sichuan−Yunnan block.

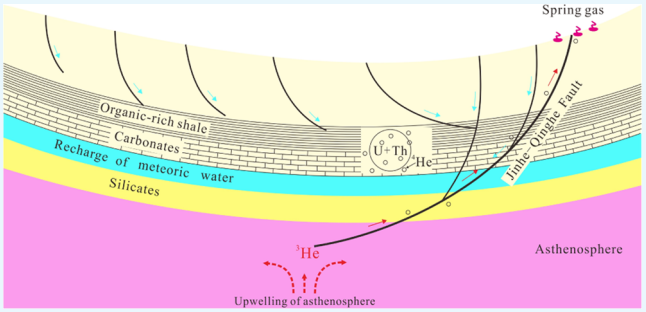

1. INTRODUCTION

In recent years, extensive reports and studies have been conducted on the geochemical characteristics of geothermal fluids in the southeastern margin of the Qinghai−Tibet Plateau.[1,2] The Sichuan−Yunnan block is close to Tengchong, Ning'er, and Pingbian volcanic fields in the southeastern margin of the Qinghai−Tibet Plateau. However, there are relatively few reports of noble gas and carbon isotopes of the geothermal fluids in the Sichuan−Yunnan block. The $^3He/^4He$ value between crustal helium ($\sim10^{-8}$) and mantle-derived helium ($\sim10^{-5}$) has a remarkable difference.[3] Unlike rocks, natural fluids can integrate helium isotope ratios of mantle-derived and crustal-derived helium to varying degrees. Therefore, the $^3He/^4He$ ratio in fluids provides a possibility to indicate local to regional geological characteristics.[4] Mantle volatiles are released through fractures and volcanic pipes connecting the mantle and the surface of the earth.[5] When mantle fluids are ejected from the subsurface through hot spring, they can be blended with crustal fluids in faults or volcanic channels.[1] In structurally stable regions, helium is formed by α decay of uranium and thorium series elements, while active extension or young volcanism areas are characterized by mantle-derived helium.[4] Therefore, the overflow of mantle-derived fluids is mainly controlled by tectonism. The $^3He/^4He$ ratio has a significant positive correlation with the deformation rate of active crust.[6] Therefore, the $^3He/^4He$ ratio is usually used to track mantle-derived materials.[7] In addition, the correlation between the carbon isotopes of CO_2 and CH_4 and the abundance of ^3He

Received: August 19, 2021
Accepted: October 22, 2021
Published: November 3, 2021

https://doi.org/10.1021/acsomega.1c04533
ACS Omega 2021, 6, 30674−30685

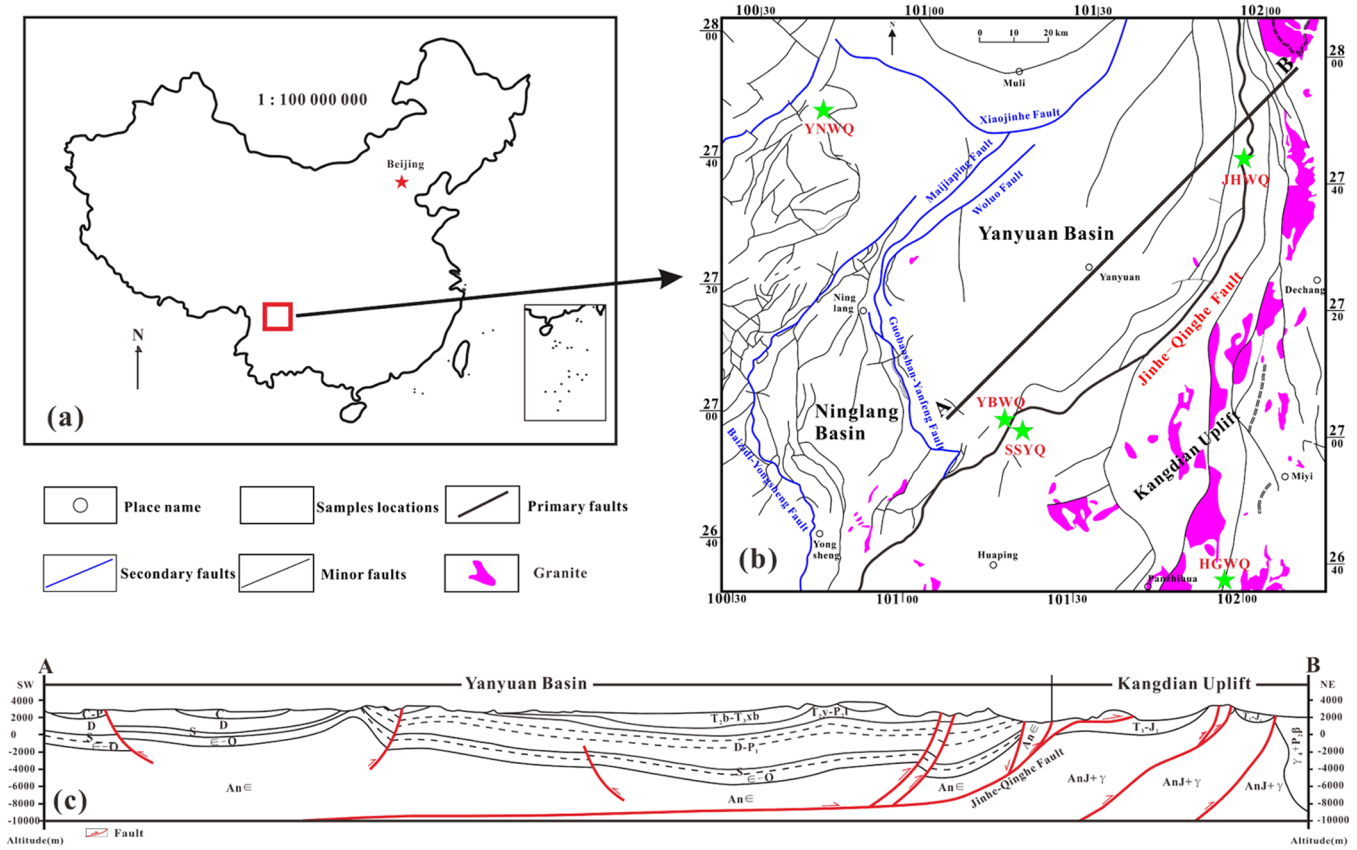

Figure 1. Location and geologic map of the Sichuan−Yunnan block, PR China. (a) Location of the study area in China; (b) sketch of geological tectonics and distribution of thermal springs in the Sichuan−Yunnan block in China; (c) stratigraphic and fault distribution of sections A−B. An∈: Precambrian; ∈-O: Cambrian-Ordovician; S: Silurian; D: Devonian; C: Carboniferous; C-P: Carboniferous-Permian; D-P_1: Devonian-Lower Permian; $P_2\beta$: Permian Emeishan basalt; T_2y-P_2l: Middle Triassic Yantang formation-Middle Permian Leping formation; T_2b-T_3xb: Middle Triassic Baishan formation-Upper Triassic Xiaboda formation; T_3-J_1: Upper Triassic−Lower Jurassic; γ_4+$P_2\beta$: Diabase + Permian Emeishan basalt; AnJ + γ: Pre-Jurassic + Granite.

can indicate geochemical information related to their sources and carbon cycle.

To discuss the mantle degassing mechanism in an intraplate tectonic environment, this paper studies the noble gas and carbon isotopic distributions of the geothermal fluids in the Sichuan−Yunnan block. By defining the relationship between the $^3He/^4He$ ratio and the abundance of main gases and carbon isotope data in the subsurface geothermal fluids, the correlation between the mantle degassing mechanism, tectonics, and magmatism is summarized.

2. GEOLOGICAL SETTINGS

The study area is located at the intersection of Yunnan and Sichuan Provinces, PR China and is geologically situated in the Sichuan−Yunnan block in China (Figure 1a). It is a part of the Yanyuan−Lijiang platform fold belt in the western margin of the upper Yangtze block.[8] It is adjacent to Sanjiang structural belt in the west and Kangdian ancient land in the east.[8] Ninglang-Yanyuan Basin is distributed in the study area (Figure 1b). The tectonic location of the Ninglang-Yanyuan Basin is a part of the southwest margin of the upper Yangtze block, which is mainly surrounded by the Jinhe-Qinghe fault, Xiaojinhe fault, Maijiaping fault, Guobaoshan-Yanfeng fault, Woluo fault, and Baizidi-Yongsheng fault.[8] The basement is the Proterozoic stratum, on which the Sinian, Lower Cambrian, Lower Ordovician−Lower Jurassic, and Paleogene sedimentary strata are deposited, missing the Middle-Upper Cambrian and Jurassic−Middle Cretaceous and Neogene, and the sedimentary stratum is more than 5000−10 000 m thick.[9] Carbonate rocks (limestone, marble, and dolomite) are developed in the Upper Sinian, Middle-Upper Ordovician, Middle-Upper Silurian, Middle-Upper Devonian, Carboniferous, Permian Maokou formation, the upper of Middle Triassic, and the lower of Upper Triassic.[10] The upper wall of the Jinhe-Qinghe thrust fault is the Sinian stratum, while the footwall is the Upper Triassic−Lower Jurassic strata in the Kangdian ancient land, and the upper wall of other faults is the Permian stratum and the footwall is the Triassic stratum in the other study areas.[8] The study area mainly developed the Jinning, Caledonian Early Hercynian, late Hercynian, Indosinian, and Yanshanian magmatism.[10] Except that the Late Permian Emeishan basalt of the Hercynian period erupted in a large area and had a huge thickness, other magmatic activities were mainly intrusive in the study area.[10] The magmatic rocks in the Kangdian uplift and surrounding areas have high U and Th contents.[11,12]

3. SAMPLES AND ANALYTICAL METHODS

Two free gases (YNWQ, YBWQ) and three dissolved gases (JHWQ, SSYQ, and HGWQ) were collected from the Sichuan−Yunnan block, China, in August 2020. The free gas is collected by a gas drainage method using a 500 mL glass bottle with a funnel on the mouth and then sealed with a rubber cap under water when the gas occupies about one-half

https://doi.org/10.1021/acsomega.1c04533
ACS Omega 2021, 6, 30674−30685

of the volume of the glass bottle. The dissolved gas adopts the same glass bottle and rubber cap to start sampling when the hot spring water flows out of the spring mouth within 10 min to avoid air pollution and ensure temperature balance. When the glass bottle is filled with hot spring water, it is sealed under water with a rubber cap. YNWQ is close to the Xiaojinhe fault; YBWQ, JHWQ, and SSYQ are located in the Jinhe-Qinghe fault; and HGWQ is sited in the Kangdian uplift. Chemical compositions and carbon and noble gas isotopes were analyzed in the Key Laboratory of Petroleum Resources of Gansu Province, China.

Chemical compositions were analyzed by a GC-9560-PDD gas chromatography (GC) instrument with a relative standard deviation of <5%, installed with a Porapak Q (2 m × 1.60 mm) column using He as the carrier gas. The oven temperature was programmed as follows: the initial temperature was set at 100 °C and maintained for 5 min and then the temperature was increased to 240 °C at 10 °C min^{-1} and maintained for 12 min. The detector temperature was 250 °C.[13]

The carbon isotopes of spring gas were tested by a 6890A GC instrument linked to a Finnigan MAT Delta Plus XP mass spectrometer.[14] The hydrocarbon compounds and CO_2 can be separated by an HP-PLOT column using He as the carrier gas. The GC oven temperature was programmed as follows: the initial temperature was set at 35 °C and maintained for 3 min, increased to 80 °C at 8 °C min^{-1}, and then to 260 °C with 5 °C min^{-1}, maintained for 10 min. The individual compounds were oxidized to CO_2 in a high-temperature (940 °C) oxidation furnace (an oxidation ceramic microreactor loaded with twisted wires) and detected by a Delta Plus XP isotope mass spectrometer with uncertainties of ±0.5‰.[14] The values of $\delta^{13}C$ are reported relative to V-PDB (Vienna Pee Dee Belemnite) in per mill.[15]

Noble gas contents and isotope compositions were measured by a Noblesse SFT noble gas mass spectrometer.[16] The analysis system is divided into four parts: sample introduction, sample purification, noble gas separation, and noble gas testing.[17] The detailed processes of sample introduction are described in the refs 14, 16. The gas was purified first using a spongy titanium furnace at 800 °C to remove active gases (H_2O, hydrocarbons, CO_2, N_2, O_2, etc.). H_2 in the gas can be eliminated by Zr−Al getters running at room temperature. Purified noble gases were separated by a cryogenic trap (10−475 K) filled with activated charcoal. He, Ne, Ar, Kr, and Xe were released for analysis at the cryogenic trap temperatures of 15, 50, 100, 150, and 230 K, respectively. The details of analytical procedures were described in ref 16. ^4He, ^{20}Ne, ^{22}Ne ^{40}Ar, and ^{36}Ar were examined with a Faraday collector, and ^3He, ^{21}Ne, ^{38}Ar, Kr, and Xe isotopes were analyzed with an electron multiplier. Experimental uncertainties for the noble gas concentrations were <10%.[16] The details of data correction are described in refs 18, 19.

4. RESULTS

4.1. Chemical Compositions and Carbon Isotopes.

The basic information and chemical compositions of the hot spring gases collected from the Sichuan−Yunnan block are presented in Table 1. These hot spring gases are dominated by N_2, which is present at a concentration ranging from 67.05 to 97.13%. This N_2-dominant hot spring gas differs from the CO_2-rich hot spring gas discovered in Tengchong[20] and Wudalianchi volcanic areas.[21] The O_2 content in HGWQ hot spring gas (9.80%) is higher than those in the other hot spring

Table 1. Chemical Compositions and Carbon Isotopes of Hot Spring Gases in the Sichuan−Yunnan Block[a]

					chemical composition (%)					carbon isotopes (‰)				
no.	sampling site	longitude (E°)	latitude (N°)	T (°C)	N_2	CO_2	O_2	CH_4	H_2	$\delta^{13}C(CO_2)$	$\delta^{13}C(CO_2)_o$	$\delta^{13}C(CH_4)$	$CO_2/^3He$	$CH_4/^3He$
1	YNWQ	100.704255	27.812170	52	84.84	12.77	1.37	0.12	0.0002	−9.0	−8.3	−19.4	1.49×10^9	1.40×10^7
2	YBWQ	101.265715	27.009167	42	67.05	30.92	1.02	0.10	0.0002	−5.0	−4.1	15.8	1.30×10^9	4.20×10^6
3	JHWQ	101.955357	27.712511	38	93.85	0.33	4.62	0.11	0.0005	−18.9	−13.5	−6.2	1.65×10^8	5.52×10^7
4	SSYQ	101.351221	26.971885	16	97.13	1.45	0.27	0.11	0.0032	−21.6	−18.6		5.05×10^8	3.83×10^7
5	HGWQ	101.951365	26.529469	57	87.88	0.09	9.80	1.24	0.0003	−26.3	−12.4	−40.9	3.48×10^6	4.79×10^7

[a]Note: The value of $\delta^{13}C(CO_2)$ is measured using the samples. $\delta^{13}C(CO_2)_o$ is the original value of $\delta^{13}C(CO_2)$.

https://doi.org/10.1021/acsomega.1c04533
ACS Omega 2021, 6, 30674−30685

gases (0.27−4.62%). However, CO_2 contents in YNWQ and YBWQ hot spring gases (12.77 and 30.92%, respectively) are higher than those in the other hot spring gases (0.09−1.45%). In addition, O_2 and CO_2 contents in N_2-rich hot spring gases are higher than those in the other major components (Table 1). The N_2/O_2 ratios (8.97−359.74) in the N_2-dominant gas are greater than N_2/O_2 ratios (3.71) in the atmosphere (Table 1). The contents of H_2 and CH_4 are very low (2−32 ppm and 0.10−1.24%, respectively) in these N_2-dominant hot spring gases.

The $\delta^{13}C(CO_2)$ values analyzed using YNWQ and YBWQ hot spring gases (−9.0 and −5.0‰, respectively) are higher than other hot spring gases (−26.3 to −18.3‰) (Table 1). The $\delta^{13}C(CO_2)_o$ values calculated by the Rayleigh fractionation in YNWQ and YBWQ hot spring gases (−8.3 and −4.1‰, respectively) are higher than other hot spring gases (−18.6 to −12.4‰) (Table 1). CO_2 contents and the $\delta^{13}C$ values of CO_2 (Table 1) exhibit a positive correlation, indicating enriched ^{13}C and depleted ^{12}C with an increase of CO_2 contents. The $\delta^{13}C(CO_2)$ values and CO_2 concentrations in YNWQ and YBWQ hot spring gases are more than −10‰ and 10%, respectively, indicating an inorganic origin.[22] However, the $\delta^{13}C(CO_2)$ values and CO_2 concentrations in other hot spring gases are less than −10‰ and 10%, respectively, indicating a predominantly organic origin.[22] The $\delta^{13}C$ values of CH_4 in YNWQ, YBWQ, JHWQ, and HGWQ are −19.4, 15.8, −6.2, and −40.9‰, respectively.

4.2. Noble Gases. *4.2.1. Helium.* ^4He contents in YNWQ, YBWQ, and HGWQ hot spring gases (850, 528, and 1649 ppm, respectively) are higher than those in JHWQ and SSYQ hot spring gases (33 and 54 ppm, respectively) (Table 2). ^4He concentrations in all samples are higher than that in the atmosphere (5.24 ppm),[23] indicating the contribution of helium mainly from nonatmospheric sources. The measured $^3He/^4He$ ratio of all samples are 0.072−0.616 R_a ($R_a = 1.4 \times 10^{-6}$).[24] To eliminate the contamination of atmospheric helium, $^3He/^4He$ ratios are air-corrected assuming atmospheric origin for ^{20}Ne. The R_c values range from 0.068 to 0.541 R_a, which is greater than crustal-derived (0.02 R_a) but much lower than mantle-derived (8 R_a) values.[3] Based on a ternary mixture model,[25] three end-members of atmospheric, crustal, and mantle-derived were used to estimate the contribution percentages of atmospheric helium (He_A), crustal helium (He_C), and mantle-derived helium (He_M) to the helium in hot spring gases. The detailed method is listed in Table 2 footnote. The calculated results show that the contribution percentages of He_A, He_C, and He_Mrange 0.33−16.14, 78.2−98.9, and 30.74−5.67%, respectively. These results suggest the significant contribution of crustal helium to the hot spring gases in the study area.

4.2.2. Neon. The contents of ^{20}Ne in hot spring gases range from 9 to 19 ppm (Table 2). In Figure 2, the $^{20}Ne/^{22}Ne$ ratios ranging from 10.3 to 10.6 in YNWQ, YBWQ, and HGWQ hot spring gases show slight deviations from the atmospheric $^{20}Ne/^{22}Ne$ ratios (9.8)[26] and are lower than mantle $^{20}Ne/^{22}Ne$ ratios (12.5).[27] However, $^{20}Ne/^{22}Ne$ ratios in JHWQ and SSYQ hot spring gases (9.8 and 9.9, respectively) are similar to the atmospheric $^{20}Ne/^{22}Ne$ ratios (9.8).[26] The $^{21}Ne/^{22}Ne$ values (0.0281−0.0328) of the hot spring gases vary from the atmospheric and crust values of $^{21}Ne/^{22}Ne$ = 0.029 and 0.03−0.70, respectively.[28] The $^{21}Ne/^{22}Ne$ values of the hot spring gases are less than 0.029 except for YNWQ spring gas, indicating that ^{21}Ne in these hot spring gases is mainly derived

Table 2. Noble Gas Contents and Their Isotope Ratios in Hot Spring Gases in the Sichuan−Yunnan Block[a]

no.	sampling site	^4He (ppm)	^{20}Ne (ppm)	^{40}Ar (ppm)	$^3He/^4He$	err (1σ)	$^{20}Ne/^{22}Ne$	err (1σ)	$^{21}Ne/^{22}Ne$	err (1σ)	$^{40}Ar/^{36}Ar$	err (1σ)	R/R_a	R_c/R_a	$^4He/^{20}Ne$	He_A (%)	He_M (%)	He_C (%)
1	YNWQ	850	11	1054	1.01×10^{-7}	1.1×10^{-8}	10.32	0.41	0.0328	0.0061	498.0	2.2	0.072	0.068	80.7	0.36	0.74	98.9
2	YBWQ	528	9	1170	4.51×10^{-7}	3.4×10^{-8}	10.45	0.19	0.0294	0.0006	317.8	2.0	0.322	0.318	57.3	0.52	3.90	95.6
3	JHWQ	54	17	1094	3.72×10^{-7}	1.1×10^{-8}	9.90	0.01	0.0278	0.0004	314.9	0.6	0.265	0.186	3.25	9.76	2.02	88.2
4	SSYQ	33	17	1095	8.62×10^{-7}	2.0×10^{-8}	9.78	0.01	0.0281	0.0002	310.8	0.5	0.616	0.541	1.97	16.14	5.67	78.2
5	HGWQ	1649	19	908	1.57×10^{-7}	5.8×10^{-9}	10.63	0.05	0.0281	0.0011	610.2	4.9	0.112	0.109	88.2	0.33	1.25	98.4

[a]Note: R/R_a is the measured $^3He/^4He$ ratio divided by that of the air ($R_a = 1.4 \times 10^{-6}$).[24] R_c/R_a is the air-corrected $^3He/^4He$ ratio. $R_c/R_a = (R/R_a - X)/(1 - X)$, $r = (^4He/^{20}Ne)_{air}/(^4He/^{20}Ne)_{sample}$, where $(^4He/^{20}Ne)_{air} = 0.318$.[25] He_A, He_M, He_C represent the proportion of Helium from air, mantle, and crust, respectively. The calculation formula is as follows: $(R_c/R_a)_{sample} = A \times (R/R_a)_{air} + M \times (R/R_a)_{mantle} + C \times (R/R_a)_{crust}$, $1/(^4He/^{20}Ne)_{sample} = A/(^4He/^{20}Ne)_{air} + M/(^4He/^{20}Ne)_{mantle} + C/(^4He/^{20}Ne)_{crust}$, $1 = A + M + C$,[25] where $(R/R_a)_{air} = 1$, $(R/R_a)_{mantle} = 8\ R_a$,[34] $(R/R_a)_{crust} = 0.02\ R_a$,[35] $(^4He/^{20}Ne)_{air} = 0.318$, $(^4He/^{20}Ne)_{mantle} = (^4He/^{20}Ne)_{crust} = 1000$.[25]

https://doi.org/10.1021/acsomega.1c04533
ACS Omega 2021, 6, 30674−30685

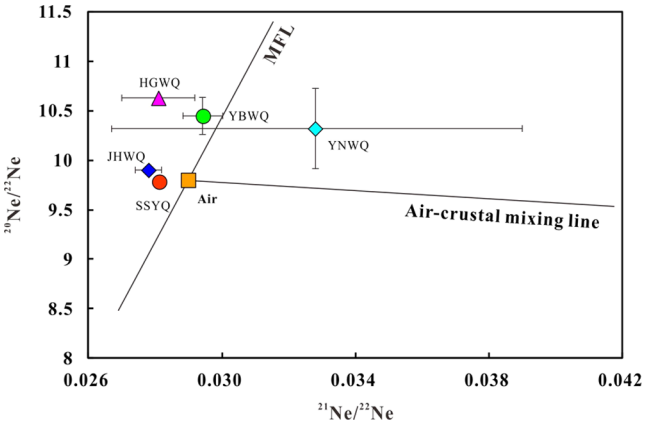

Figure 2. Plot of $^{20}Ne/^{22}Ne$ ratios vs $^{21}Ne/^{22}Ne$ ratios. The Ne isotopic pattern can be accounted for by the crustal ^{21}Ne addition to the air ratio and a mass fraction-related process. The $^{20}Ne/^{22}Ne$ and $^{21}Ne/^{22}Ne$ values for atmospheric and crustal were from refs 26, 29, respectively. Although the error of the $^{21}Ne/^{22}Ne$ ratio in YNWQ is 0.0061, it can still be explained by the mixing of mass fractionation and the crustal ^{21}Ne addition to the air ratio. MFL, mass fractionation line. Samples that do not show the error bars indicate 1σ uncertainties are smaller than symbols.

from the atmosphere without evident crustal addition of ^{21}Ne. Previously reported data also show the same isotopic pattern.[30] All of the Ne isotopic ratios can be accounted for by two processes: one is variable crustal radiogenic ^{21}Ne addition to the air Ne, and the other is the mass fractionation process (Figure 2).

4.2.3. Argon. ^{40}Ar contents in the hot spring gases are 908–1170 ppm, and $^{40}Ar/^{36}Ar$ ratios vary between 310.8 and 610.2 (Table 2). In Figure 3, $^{40}Ar/^{36}Ar$ ratios of the hot spring gases

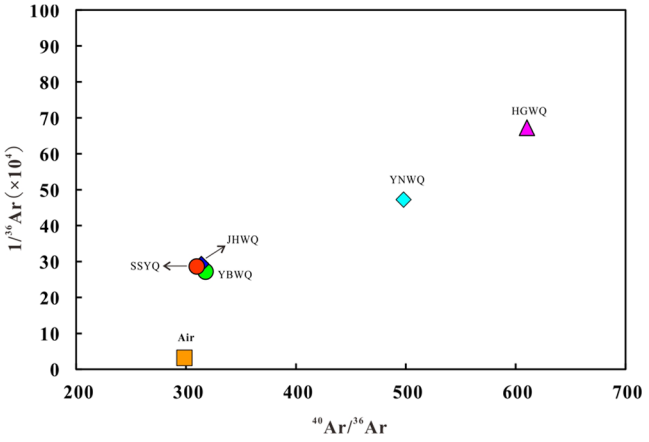

Figure 3. Plot of $1/^{36}Ar$ ratios vs $^{40}Ar/^{36}Ar$ ratios. Atmospheric values of $1/^{36}Ar$ = 3.18 and $^{40}Ar/^{36}Ar$ = 298.[31] The proportion of excess $^{40}Ar^*$ to total ^{40}Ar is negatively correlated with atmospheric ^{36}Ar. 1σ uncertainties are smaller than symbols.

are higher than the atmospheric $^{40}Ar/^{36}Ar$ ratios (298).[31] Because of the minor mantle contribution proved by the $^{3}He/^{4}He$ ratio, therefore, excess ^{40}Ar generally was derived from radioactive decay of ^{40}K in the crust. Based on excess $^{40}Ar^* = {}^{40}Ar - 296.0 \times {}^{36}Ar$,[32] the proportion of excess $^{40}Ar^*$ to total ^{40}Ar is 40.56 and 51.49% in YNWQ and HGWQ hot spring gases, respectively, and 6.86, 5.99, and 4.78% in YBWQ, JHWQ, and SSYQ hot spring gases, respectively.

5. DISCUSSION

5.1. Correlation between ^{4}He, ^{20}Ne, and N_2 Contents in Hot Spring Gases. The contents of ^{20}Ne and ^{4}He show a positive correlation in hot spring gases except for SSYQ and JHWQ samples in the Sichuan–Yunnan block (Figure 4a). ^{20}Ne is almost completely derived from the atmosphere and enters the subsurface by dissolving in groundwater.[33] ^{4}He is formed by α decay of uranium and thorium series elements.[33] Generally, there is no correlation between ^{4}He and ^{20}Ne from different sources, and they are also subject to variable dilution of main gas components in the later stage. The positive correlation between ^{4}He and ^{20}Ne in the sample indicates that ^{4}He and ^{20}Ne have mixed before the main gas component is charged. In addition, this correlation provides direct evidence of the important role of groundwater in the enrichment process of crustal-derived gas. Similar relationships exist between $^{4}He/N_2$ and $^{20}Ne/N_2$ (Figure 4b) and N_2 and ^{4}He concentrations (Figure 4c), implying a common trapping mechanism for ^{4}He, ^{20}Ne, and N_2 in the geothermal fluids. Notably, ^{4}He vs ^{20}Ne, ^{4}He vs N_2, and $^{4}He/N_2$ and $^{20}Ne/N_2$ show two trend distributions in the hot spring gases; this is may be caused by the difference in ^{4}He contents in the spring gases. The difference of ^{4}He contents in the samples is mainly determined by the difference of U and Th concentrations in rocks in different regions. This also shows that the U and Th contents of rocks in SSYQ and JHWQ areas are lower than those in other sample distribution areas. However, ^{20}Ne vs N_2 shows only one trend (Figure 4d), indicating that ^{20}Ne and N_2 have the same source and geological migration pathway.

5.2. Origins of Gases Discharging from the Sichuan–Yunnan Block. *5.2.1. N_2–Ar–He System.* The magma fluids, crustal fluids, and atmospheric precipitation fluids have different distribution positions in N_2–Ar–He triangle diagram; therefore, the N_2–Ar–He triangle diagram is usually used to determine the source of the subsurface fluids.[36,37] The N_2, He, and Ar contents of the three major sources of gas usually have the following distribution characteristics (Figure 5). The air and air-saturated water (ASW) usually have lower He contents, and N_2/Ar ratios are 83 and 38, respectively. However, mantle-sourced gases usually have higher He contents and lower N_2 contents, with N_2/He less than 200.[38] Arc-type gases usually have high N_2 contents, N_2/He greater than 1000, and N_2/Ar greater than 200. The hot spring gases from the Sichuan–Yunnan block are distributed along between mantle–crustal-derived and air or ASW in Figure 5, and the N_2/Ar values of samples are greater than that of air (83), except for the YBWQ hot spring gas, the N_2/Ar ratio is 77 between air (83) and ASW (38). The excessively high N_2/Ar ratio may be caused by excessive N_2 addition or N_2/Ar fractionation during the fluid migration process.[39] Compared with the hot spring gases from the Sichuan–Yunnan block, Tengchong and Wudalianchi gases show mantle–crustal-derived and air or ASW distribution, but Tengchong and Wudalianchi gases have higher mantle He and Ar concentrations. In addition, some Tengchong gases fall along the arc-type gas region.

5.2.2. Helium in Hot Spring Gases. Due to the different isotopic compositions of noble gases in the different geospheres, $^{4}He/^{20}Ne$ and $^{3}He/^{4}He$ can further reveal deep material information and the source of gas components.[43] As shown in Figure 6, a simple ternary mixture model including atmospheric (R_a), mantle (~8.0 R_a), and crustal (0.02 R_a) can be used to indicate the source of geothermal fluids in the

https://doi.org/10.1021/acsomega.1c04533
ACS Omega 2021, 6, 30674–30685

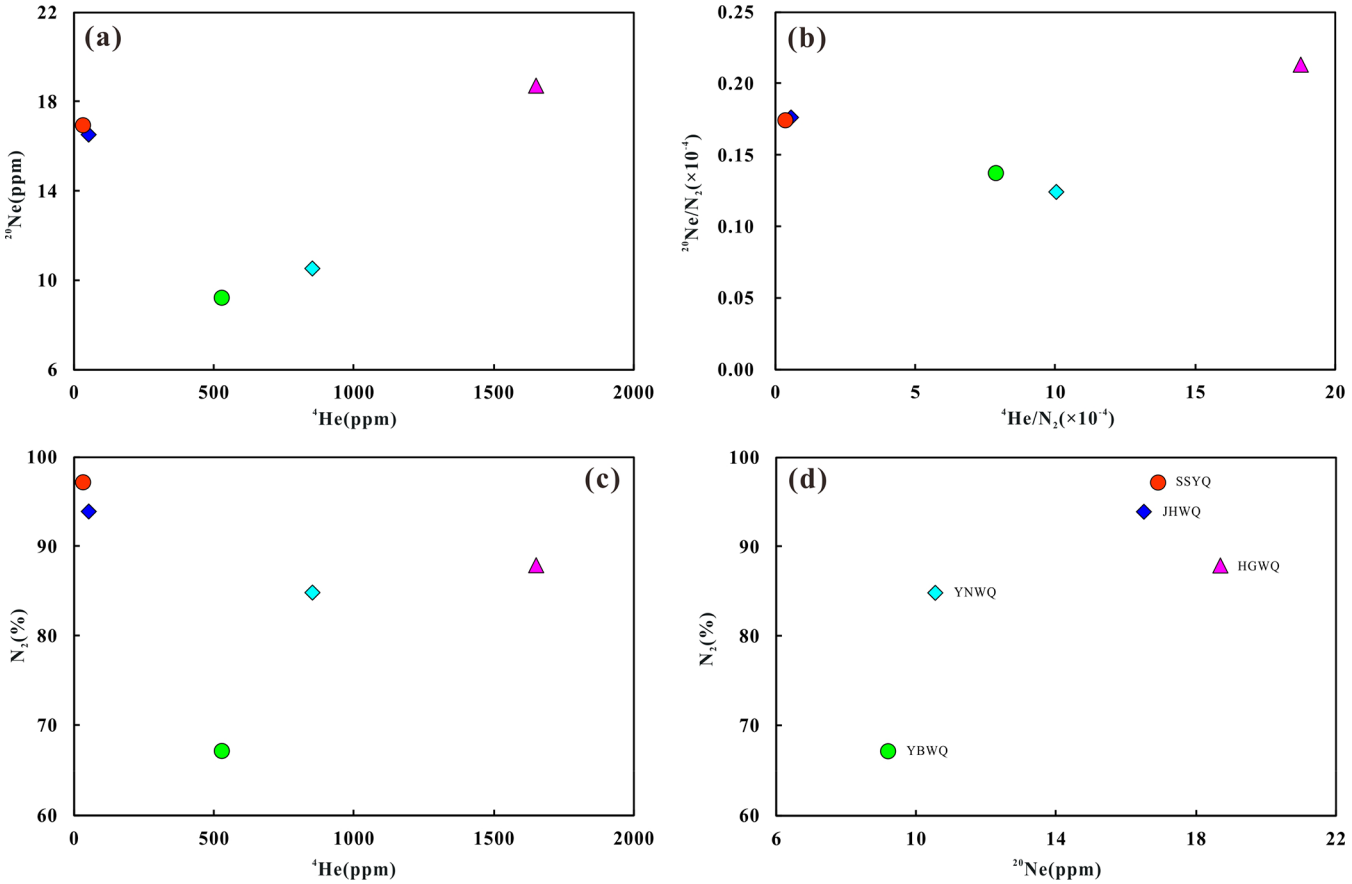

Figure 4. Plots of (a) ^{4}He vs ^{20}Ne content, (b) ^{4}He/N$_2$ vs ^{20}Ne/N$_2$, (c) ^{4}He vs N$_2$ content, and (d) ^{20}Ne vs N$_2$ concentration indicating the strong correlation between ^{4}He, ^{20}Ne, and N$_2$ contents.

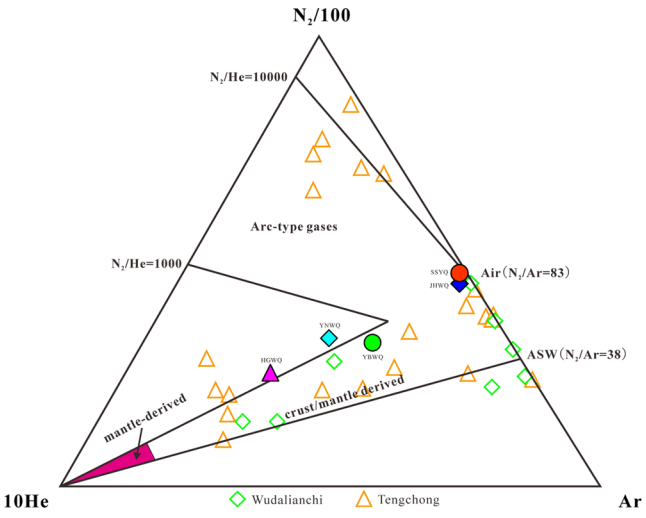

Figure 5. N$_2$−Ar−He ternary diagram. Modified from ref 40. Wudalianchi data from ref 41; Tengchong data from ref 42. The hot spring gases from the Sichuan−Yunnan block are distributed along between mantle−crustal-derived and air or ASW.

Sichuan−Yunnan block.[25] The ^{4}He/^{20}Ne values range from 57.32 to 88.18 except for JHWQ and SSYQ hot spring gases with values of 3.25 and 1.97, respectively, and R_c/R_a ratios (0.068−0.541 R_a) all are less than 0.6 R_a. It can be clearly seen that all hot spring gases in the Sichuan−Yunnan block are scattered between air and crustal mixing lines. Therefore, all the hot spring gases are typical of a crustal origin. Usually, ^{3}He/^{4}He ratios of natural gases are greater than 0.1 R_a, suggesting the presence of mantle He components.[44] The proportion of mantle He in YBWQ, JHWQ, and SSYQ hot spring gases are 3.90, 2.02, and 5.67%, respectively, and this result is consistent with the Jinhe-Qinghe fault cut through the lower crust.[45] However, the proportion of mantle He in the YNWQ and HGWQ hot spring gases (0.74 and 1.25%, respectively) are relatively lower than that in the hot spring gases located in the Jinhe-Qinghe fault.

In addition, Wudalianchi, Changbai Mountain, and Tengchong hot spring gases are also plotted in Figure 6 for comparison. All Wudalianchi and Changbai Mountain hot spring gas ^{3}He/^{4}He values are greater than 1.0 R_a, indicating that these spring gases are mainly derived from the mantle origin. The hot spring gases from Tengchong, Yunnan Province can be divided into CO$_2$- and N$_2$-rich gases.[4] Generally, N$_2$-rich gases have a higher crust source gas input, and CO$_2$-rich gases have a higher mantle source gas input.[46]

5.2.3. CO$_2$ and CH$_4$ in Hot Spring Gases. The δ^{13}C values of carbonaceous compounds in the hot spring gases contain abundant geochemical information. Generally, the different sources of CO$_2$ have different carbon isotope distribution characteristics. The δ^{13}C value of CO$_2$ with the range of −10 to 0‰ and the CO$_2$ contents greater than 15% can be regarded as an inorganic origin.[22] However, CO$_2$ contents and the δ^{13}C values of CO$_2$ less than 10 and −10‰, respectively, can be regarded as an organic origin.[48] The δ^{13}C value of CO$_2$ is less than −14‰, which generally indicates the source of

https://doi.org/10.1021/acsomega.1c04533
ACS Omega 2021, 6, 30674−30685

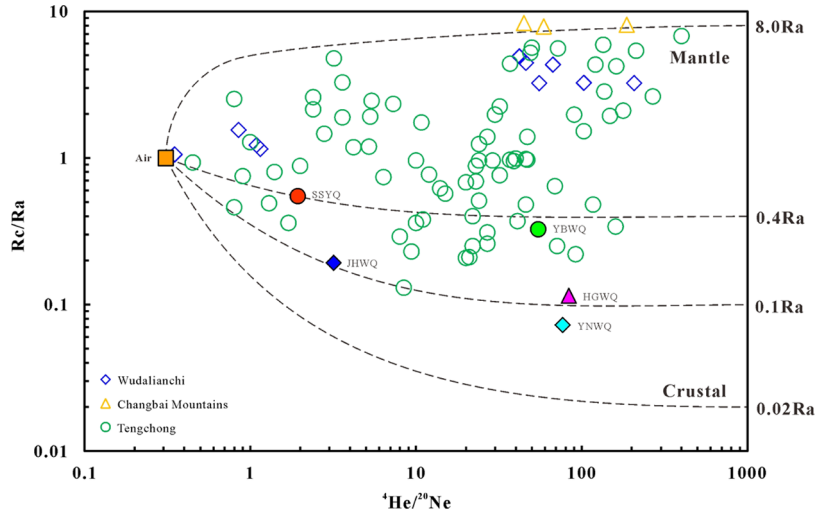

Figure 6. Plot of R_c/R_a vs $^4He/^{20}Ne$ ratios. Atmospheric: $^3He/^4He = R_a$, $^4He/^{20}Ne = 0.318$; crustal-derived: $^3He/^4He = 0.02\ R_a$, $^4He/^{20}Ne = 1000$; mantle-derived: $^3He/^4He = 8\ R_a$, $^4He/^{20}Ne = 1000$.[25] All samples from the Sichuan−Yunnan block are scattered between air and crustal mixing lines, indicating helium of all of the hot spring gases is typical of a crustal origin. Wudalianchi data are from refs 41, 47; Changbai Mountains data are from ref 47 Tengchong data are from refs 46, 47.

organic matter,[49] while the $\delta^{13}C$ value of marine limestone is usually $0 \pm 3‰$.[50]

If the mantle-derived fluids are effectively mixed through the lithosphere without significant fractionation, the $CO_2/^3He$ ratio in the surface fluids is between the mantle (2×10^9) and crustal ($>10^{10}$) values.[51] For example, the samples from the Sichuan Basin and YNWQ and YBWQ spring gases have a $CO_2/^3He$ ratio between the mantle and crustal values (Figure 7). However, compared with the mantle and crustal end-

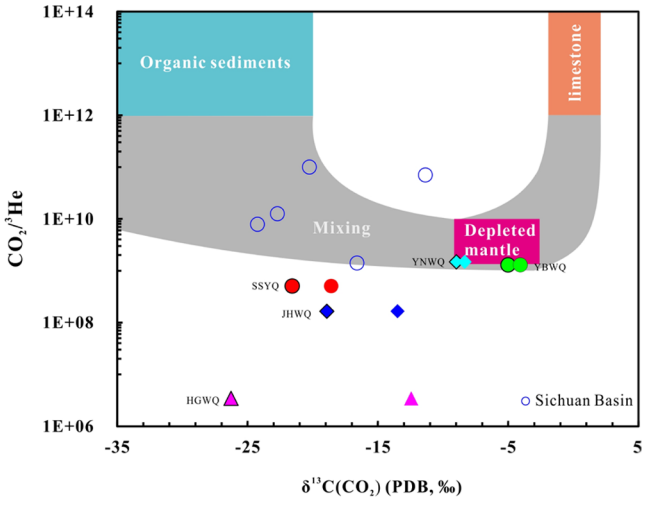

Figure 7. Plot of $\delta^{13}C(CO_2)$ vs $CO_2/^3He$. Except for YNWQ and YBWQ spring gas, other sample data plot below standard mixing fields. Ranges of different sources are from refs 52, 60. The $\delta^{13}C(CO_2)$ value of the sample with the frame is the initial value, and the $\delta^{13}C(CO_2)$ value of the sample without the frame is the correction value. Sichuan Basin data are from ref 61.

member,[52] the JHWQ, SSYQ, and HGWQ have significantly low $CO_2/^3He$ ratios (1.65×10^8, 5.05×10^8, and 3.48×10^6, respectively). ^3He production within the crust is dominated by thermal neutron capture by ^6Li in reaction $^6Li(n,\alpha)^3H$-$(\beta^-)^3He$.[53] Even if the Li content in surrounding rocks reaches 100 ppm,[54] the local $^3He/^4He$ ratio of radiogenic helium cannot exceed 0.1 R_a.[55] Thus, ^3He is mainly derived from the mantle, and it is impossible for ^3He to be added during the upward migration of gas. ^3He belongs to noble gas, and there is no correlation between the geothermal system and volcanic activity in the study area. Thus, except for dissolution, almost no process could alter ^3He concentrations in the geothermal fluids. When the gas is released from the geothermal fluids, due to the solubility difference in the aqueous solution, CO_2 and He may be fractionated.[56] Helium prefers to partition into exsolved vapor phase relative CO_2, rendering the residual phase $CO_2/^3He$ values elevated compared to the original values. The $CO_2/^3He$ ratio in the dissolved gases (JHWQ, SSYQ, and HGWQ) is lower than the bubbling gas (YNWQ and YBWQ), which is similar to the mantle $CO_2/^3He$ ratio ($1-10 \times 10^9$).[52] Therefore, hydrothermal degassing is not the cause of $CO_2/^3He$ ratio change.

In the ascending channel, calcite precipitates when the CO_2 partial pressure decreases, which leads to the decrease of $CO_2/^3He$ ratio and the $\delta^{13}C(CO_2)$ changes.[57] Based on the Rayleigh fractionation ($\delta^{13}C(CO_2) = \delta^{13}C(CO_2)_o + \varepsilon \ln f$,[58] the value of $\delta^{13}C(CO_2)$ is measured by the samples, the $\delta^{13}C(CO_2)_o$ is the original value of $\delta^{13}C(CO_2)$, f is the fraction of CO_2 remaining in the geothermal fluids, and ε is the carbon isotope fractionations for precipitation. The specific calculation method is shown in ref 59; the original value of $\delta^{13}C(CO_2)$ values ranges from −18.6 to −4.1‰. The gas plots below the crustal and mantle range in the $CO_2/^3He$-$\delta^{13}C(CO_2)$ space (Figure 7) imply the loss of CO_2 relative to He, as previously observed in numerous natural CO_2 accumulations.[59] About 83.5, 49.5, and 99.5% of CO_2 has been lost in JHWQ, SSYQ, and HGWQ, respectively, assuming mantle-derived CO_2 with a typical magmatic range of $1-10 \times 10^9$.[52] In addition, the loss contents of CO_2 reflected by the $CO_2/^3He$ values are positively correlated with the carbon isotope fractionation degree of CO_2 (Figure 7).

In Figure 8, the correlation of R_c/R_a versus $\delta^{13}C(CO_2)$ indicates that all spring gases from the Sichuan−Yunnan block are plotted within the two mixing lines (between mantle and limestone and between the mantle and organic sediments). The YNWQ and YBWQ spring gases contain 12.77 and

https://doi.org/10.1021/acsomega.1c04533
ACS Omega 2021, 6, 30674−30685

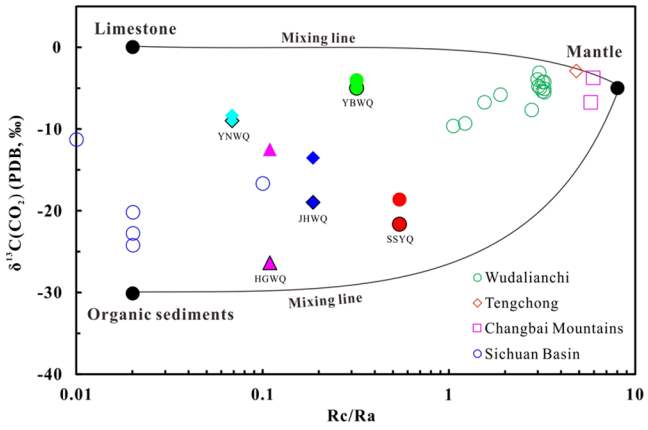

Figure 8. Plot of $\delta^{13}C(CO_2)$ vs R_c/R_a. Limestone: $\delta^{13}C(CO_2)$ = 0‰, $^3He/^4He$ = 0.02 R_a, organic sediments: $\delta^{13}C(CO_2)$ = −30‰, $^3He/^4He$ = 0.02 R_a; mantle: $\delta^{13}C(CO_2)$ = −5‰, $^3He/^4He$ = 8.0 R_a.[25] The $\delta^{13}C(CO_2)$ value of the sample with the frame is the initial value, and the $\delta^{13}C(CO_2)$ value of the sample without the frame is the correction value. All samples are distributed between the two end-members of limestone and organic sediments. Wudalianchi data are from refs 21, 41, 47; Changbai Mountains and Tengchong data are from ref 47; Sichuan Basin data are from ref 61.

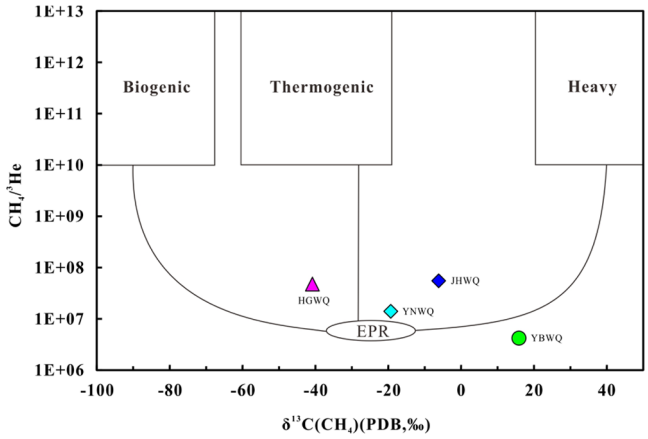

Figure 9. Plot of $\delta^{13}C(CH_4)$ vs $CH_4/^3He$. The hot spring gas has a tendency to approach the end components of the EPR (abiogenic), which suggests that microbial oxidation processes are likely to exist in geothermal systems.

30.92% CO_2, respectively, with $\delta^{13}C(CO_2)$ values of −9.0 and −5.0‰, respectively, which are overlapping that for typical magmatic CO_2. However, considering the outcrops of organic-rich shale and carbonate rocks in the Sichuan−Yunnan area[8] and the relatively low $^3He/^4He$ ratio, CO_2 is mainly contributed by limestone mixed with minor mantle and organic CO_2. The JHWQ, SSYQ, and HGWQ spring gases from the Sichuan−Yunnan block with low CO_2 contents and $\delta^{13}C(CO_2)$ values are −18.9, −21.6, and −26.3‰, respectively, which are significantly less than those for typical inorganic carbon. Therefore, the spring gas CO_2 origins in the Sichuan−Yunnan block are mainly derived from mixing of limestone and organic sediments with minor mantle CO_2. The organic-rich shale and carbonate decomposition provides organic sediments and limestone-type carbon as two end-members of the crust that pollute the rising mantle volatiles. However, the $\delta^{13}C(CO_2)$ value and the $^3He/^4He$ ratio of the samples in the Sichuan Basin are less than −10‰ and 0.02 R_a, respectively, indicating that CO_2 is mainly derived from the contribution of organic sediments CO_2 (Figure 8). In addition, the $\delta^{13}C(CO_2)$ value and the $^3He/^4He$ ratio of the samples in the Quaternary volcanos (Wudalianchi, Tengchong, and Changbai Mountains) are greater than −10‰ and 1.0 R_a, respectively, suggesting the CO_2 is mainly derived from the contribution of mantle CO_2 (Figure 8).

Generally, the formation of natural CH_4 is reported in four ways: (a) biogenic methane formed by bacteria at a temperature less than 100 °C,[62] (b) thermal decomposition of organic matter at a temperature greater than 100 °C,[63] (c) degassing of the mantle,[64] and (d) formation by chemical reactions, such as the Fischer−Tropsch synthesis reaction.[65] In Figure 9, the plot of the $\delta^{13}C(CH_4)$ versus $CH_4/^3He$ values can effectively identify the four origins of CH_4.[66] The HGWQ spring gas is located in the mixing between thermogenic methane and biogenic methane. The other spring gas methane is thermogenic methane, which tends to be a heavy carbon isotope. The hot spring gases have a tendency to approach the end components of the EPR (abiogenic) (Figure 9), which suggests that microbial oxidation processes are likely to exist in geothermal systems.[66] The microorganisms seem to preferentially consume ^{12}C in methane, resulting in the enrichment of ^{13}C in methane. Therefore, methane has a heavier carbon isotope and a decrease of $CH_4/^3He$ values in the hot spring gases from the Sichuan−Yunnan block. Compared with the other hot spring gases, the CH_4 in YBWQ spring gas may undergo the greatest impact on the degree of microbial oxidation.

5.3. Mantle Helium Distribution in an Intracontinental Crust and Its Tectonic Implications. Assuming that the upward transmission rate of helium along the stratum in the study area is equal to that in Southern California (147 mm a^{-1}),[67] it takes 4.4 Ma for helium to pass through the 40 km crust. At the same time, helium is in the whole granite (D_{He} = 5 × 10^{-7} m^2 a^{-1})[53] migration distance is only 1 mm, indicating the importance of faults for the upward transport of helium. Deep and large faults are one of the important channels through which mantle fluids pass through the crust, and the ratio of $^3He/^4He$ can reflect the rate of mantle fluids passing through fault zones.[68] Usually, $^3He/^4He$ ratio in the volcanic areas is higher than that in the areas without magmatic activity.[44] The high $^3He/^4He$ ratios are usually related to subsurface melting or magmatism.[69] The $^3He/^4He$ ratio has a significant positive correlation with the deformation rate of the active crust.[6] Therefore, the migration of mantle helium in the crust may be influenced by the scale of fault, fault activity rate, and magmatic activity in the Sichuan−Yunnan block.

The hot spring gas is mainly distributed along the fault in the Sichuan−Yunnan block. YNWQ is close to the Xiaojinhe fault, YBWQ, JHWQ, and SSYQ are close to the Jinhe-Qinghe fault, and HGWQ is located in the Kangdian uplift. The Moho depth of the Yunnan block is 50−60 km.[70,71] In addition, there is a low-velocity zone within ∼30 km in central Yunnan.[72] According to the previous structural geological profile,[70−73] the stratigraphic contact relationship on both sides of the Jinhe-Qinghe fault is that the Sinian Dengying formation (Zbd) in the north is thrust napped onto the Triassic Jurassic formation (T_3-J_1) in the south (Figure 1c). Based on the characteristics of the surface geological structure and deep electrical anomaly, it is considered that the Jinhe-Qinghe fault is a lithospheric fault passing through the Moho surface (Figure 10).[45] Therefore, the contribution ratio of mantle-derived helium of hot spring

https://doi.org/10.1021/acsomega.1c04533
ACS Omega 2021, 6, 30674−30685

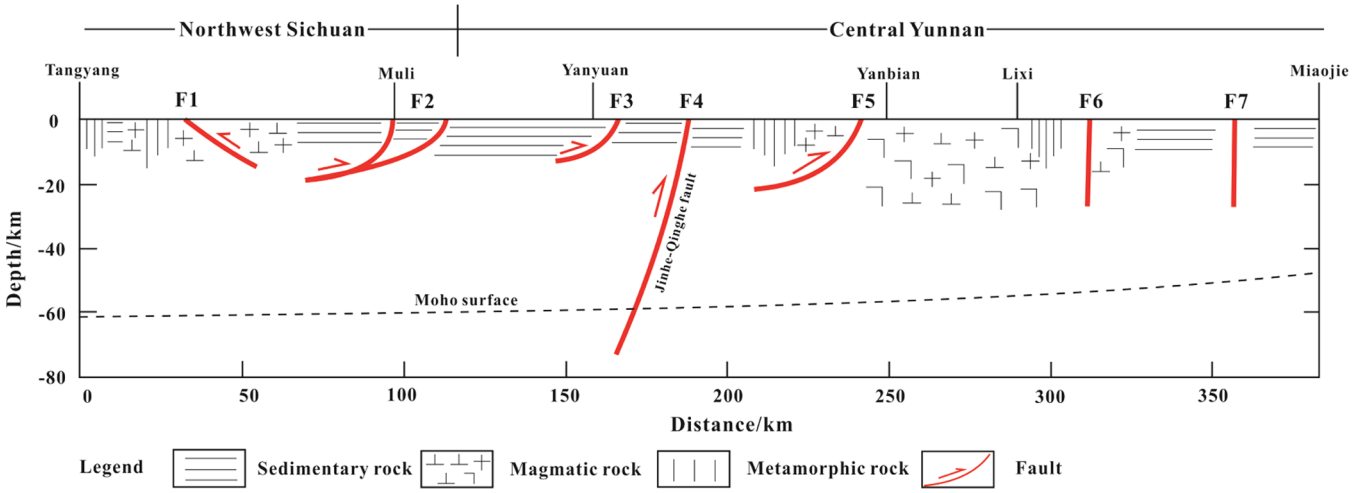

Figure 10. Distribution of structural faults in the Sichuan−Yunnan region (modified from ref 45).

gases (the proportions of mantle-derived helium in YBWQ, SSYQ, and JHWQ samples are 3.90, 5.67, and 2.02%, respectively) near the Jinhe-Qinghe fault is higher than that of hot spring gases distributed in other fault zones (the proportions of mantle-derived helium in YNWQ and HGWQ are 0.74 and 1.25%, respectively). In addition, the lower proportion of mantle-derived helium in YNWQ and HGWQ than other spring gases near the Jinghe-Qinghe fault may be caused by the smaller scale of fault around YNWQ and HGWQ than the Jinghe-Qinghe fault.

Although a large amount of mantle-derived helium exists in Tengchong, Pingbian, and Ning'er volcanic areas, there is low mantle-derived helium observed in the Sichuan−Yunnan block. Compared with the mantle-derived helium of typical intraplate volcanic areas in China, the maximum proportion of mantle-derived helium in Tengchong, Changbai Mountain, Hainan, and Wudalianchi volcanic fields can reach 65.6,[69] 80,[74] 15.6, and 38%,[4,21] respectively. However, the proportion of mantle-derived helium (0.74−5.67%) in the Sichuan−Yunnan block is significantly lower. In addition, when the mantle volatiles was transported along the deep fault in the granitic crust, the α decay of uranium and thorium series elements produces ^{4}He, which is added to mantle fluids. Therefore, the ^{3}He/^{4}He ratio in hot spring gas shows a certain functional relationship with uranium and thorium contents in rock, indicating the time of extracting ^{4}He into the fluids and passing through the crust.[75] Geochemical evidence shows that the Mesozoic granites in the Sichuan−Yunnan block have high U and Th contents.[11,12] Therefore, mantle-derived helium is diluted by the radiogenic ^{4}He produced in the crust. Besides, the slow transport of mantle-derived helium in deep faults (e.g., the average flow rate of the Karakoram fault is 19 mm a^{-1})[76] will lead to more time mixing of crustal helium and mantle-derived helium.

Fault activity and deformation have a positive correlation with the migration of mantle-derived helium in the crust. The increase of fault slip rate can significantly improve and maintain the high permeability of fault.[77] According to the statistical relationship of the helium isotope (R_a) and the strike-slip rate (mm a^{-1}) of the S-wave low-speed anomaly occurring in the 70 km deep region (^{3}He/^{4}He (R_a) = strike-slip rate of fault × 0.127 + 0.551, R_2 = 0.869),[78] the results show that the strike-slip rates of the Xiaojinhe fault, Jinhe-Qinghe fault, and Kangdian uplift are 0.10, 1.03−3.82, and 0.42 mm a^{-1}, respectively. The fault activity rate calculated by ^{3}He/^{4}He is consistent with the current activity rate characterization of main faults in the Sichuan−Yunnan region through GPS.[79] Therefore, the crustal deformation rate is positively correlated with the migration rate of mantle fluids in the crust. According to the above analysis, the low fault activity rate, the small fault scale, and the not obvious magmatic activity result in the low proportion of mantle-derived helium of the geothermal fluids in the Sichuan−Yunnan block.

6. CONCLUSIONS

The N_2-dominant component (67.05−97.13%) were observed in the hot spring gas samples. contents of the YBWQ sample (67.05%).The helium isotope of all hot spring gases shows 0.068−0.541 R_a, and the percentages of atmospheric, crustal, and mantle-derived helium range 0.33−16.14, 78.2−98.9, and 0.74−5.67%, respectively. The N_2−Ar−He triangle diagram and ^{40}Ar/^{36}Ar ratios indicate that N_2 and Ar are mostly meteoric, and YNWQ and HGWQ have more crustal-derived Ar contribution (40.56 and 51.49%, respectively). The low CO_2/^{3}He ratio (e.g., 3.48 × 10^6 in HGWQ) is probably accused by the loss of CO_2 by calcite precipitation. The $\delta^{13}C(CO_2)_o$ values calculated by Rayleigh fractionation and the CO_2 concentrations suggest that YNWQ and YBWQ are consistent with the inorganic origin and JHWQ, SSYQ, and HGWQ are consistent with the organic origin. The plot of R_c/R_a versus $\delta^{13}C(CO_2)_o$ indicates that the spring gas CO_2 origin in the Sichuan−Yunnan block is mainly derived from mixing of limestone and organic sediments with minor mantle CO_2. The $\delta^{13}C(CH_4)$ versus CH_4/^{3}He values indicate that the origin of methane is thermogenic and microbial oxidation. Mantle helium contents in YBWQ, SSYQ, and JHWQ samples near the Jinhe-Qinghe fault are 3.90, 5.67, and 2.02%, respectively, and higher than those in hot spring gases distributed in other fault zones (mantle helium contents in YNWQ and HGWQ are 0.74 and 1.25%, respectively). Such distribution patterns and low mantle-derived helium proportions are most likely controlled by the low fault activity rate, the small fault scale, and not obvious magmatic activity in the Sichuan−Yunnan block.

https://doi.org/10.1021/acsomega.1c04533
ACS Omega 2021, 6, 30674−30685

AUTHOR INFORMATION

Corresponding Authors

Shixin Zhou − *Northwest Institute of Eco-Environment and Resources, Chinese Academy of Sciences, Lanzhou 730000, China; Key Laboratory of Petroleum Resources, Gansu Province, Lanzhou 730000, China*; Email: sxzhou@lzb.ac.cn

Jing Li − *Northwest Institute of Eco-Environment and Resources, Chinese Academy of Sciences, Lanzhou 730000, China; Key Laboratory of Petroleum Resources, Gansu Province, Lanzhou 730000, China*; Email: lj1926@lzb.ac.cn

Authors

Bingkun Meng − *Northwest Institute of Eco-Environment and Resources, Chinese Academy of Sciences, Lanzhou 730000, China; Key Laboratory of Petroleum Resources, Gansu Province, Lanzhou 730000, China; University of Chinese Academy of Sciences, Beijing 100049, China*; orcid.org/0000-0003-4006-9099

Zexiang Sun − *Northwest Institute of Eco-Environment and Resources, Chinese Academy of Sciences, Lanzhou 730000, China; Key Laboratory of Petroleum Resources, Gansu Province, Lanzhou 730000, China; University of Chinese Academy of Sciences, Beijing 100049, China*

Complete contact information is available at: https://pubs.acs.org/10.1021/acsomega.1c04533

Notes

The authors declare no competing financial interest.

ACKNOWLEDGMENTS

The authors are very grateful to the Associate Editor Dr. Mohamed Mahmoud and three anonymous reviewers for their constructive comments and suggestions, which greatly improved the professionalism and standardization of the manuscript. This study was supported by the National Science and Technology Projects of Ministry of Science and Technology of China (No. 2016ZX05003002004), the National Natural Science Foundation of China (Nos. 41072105 and 41872147), and the Project of Exploration Branch of China Petrochemical Corporation "Research on Geological Conditions of Helium Accumulation and Block Optimization in Peripheral Areas of the South China" (No. 35450003-20-ZC0607-0014).

REFERENCES

(1) Zhang, L.; Guo, Z.; Sano, Y.; Zhang, M.; Sun, Y.; Cheng, Z.; Yang, T. Flux and genesis of CO_2 degassing from volcanic-geothermal fields of Gulu-Yadong rift in the Lhasa terrane, South Tibet: Constraints on characteristics of deep carbon cycle in the India-Asia continent subduction zone. *J. Asian Earth Sci.* **2017**, *149*, 110−123.

(2) Zhou, X.; Wang, W.; Chen, Z.; Yi, L.; Liu, L.; Xie, C.; Cui, Y.; Du, J.; Cheng, J.; Yang, L. Hot Spring Gas Geochemistry in Western Sichuan Province, China After the Wenchuan Ms 8.0 Earthquake. *Terr., Atmos. Ocean. Sci.* **2015**, *26*, 361−373.

(3) Mamyrin, B. A.; Tolstikhin, I. N. *Helium Isotope in Nature*; Elsevier, 1984; p 273.

(4) Sheng, X.; Zheng, G.; Xu, Y. Helium, Argon and Carbon Isotopic Compositions of Spring Gases in the Hainan Island, China. *Acta Geol. Sin.* **2012**, *86*, 1515−1523.

(5) Rizzo, A. L.; Caracausi, A.; Chavagnac, V.; Nomikou, P.; Polymenakou, P. N.; Mandalakis, M.; Kotoulas, G.; Magoulas, A.; Castillo, A.; Lampridou, D.; Marusczak, N.; Sonke, J. E. Geochemistry of CO_2-Rich Gases Venting From Submarine Volcanism: The Case of Kolumbo (Hellenic Volcanic Arc, Greece). *Front. Earth Sci.* **2019**, *7*, No. 60.

(6) Kennedy, B. M.; van Soest, M. C. Flow of mantle fluids through the ductile lower crust: helium isotope trends. *Science* **2007**, *318*, 1433−1436.

(7) Hilton, D. R.; Porcelli, D. Noble Gases as Mantle Tracers. In *Treatise on Geochemistry*; Richard, W. C.; Heinrich, D. H.; Karl, K. T., Eds.; Elsevier Ltd: London, UK, 2003; pp 277−318.

(8) Zhang, Z.; Yang, W.; Li, X.; Song, Y.; Jiang, Z.; Luo, Q. Geochemical Characteristics of the Middle Devonian Dacaozi-Tanshanping Shale Strata in the Yanyuan Basin, Southwest China: Implications for Organic Matter Accumulation and Preservation. *Geofluids* **2021**, 1−24.

(9) He, W.; Tang, T.; Yue, M.; Deng, J.; Pan, G.; Xing, G.; Luo, M.; Xu, Y.; Wei, Y.; Zhang, Z.; Xiao, Y.; Zhang, K. Sedimentary and Tectonic Evolution of Nanhuan-Permian in South China. *Earth Sci.* **2014**, *39*, 929−953.

(10) Wang, Z.; Deng, M.; Cheng, J.; Zhang, H. Influence of Fault and Magmatism on Oil and Gas Preservation Condition, to the West of Kangdian Ancient Continent: Taking Yanyuan Basin as an Example. *Earth Sci.* **2018**, *43*, 3616−3624.

(11) Yao, J.; Li, J.; Zhou, J.; Chen, Z.; Yao, H. LA-ICP-MS zircon U-Pb dating of migmatite in Datian, Panzhihua City, and its geological significance. *Geol. Bull. China* **2017**, *36*, 381−391.

(12) Yin, M.; Xu, Z.; Song, H.; Zhang, S.; Zhang, C.; Li, T.; Tian, J. Significant geological events related to uranium mineralization in the Datian area, Xikang-Yunnan Geo-Axis. *Geol. Explor.* **2021**, *57*, 14−29.

(13) Li, L.; Liu, Y.; Wang, X.; Zhang, M.; Cao, C.; Xing, L.; Li, Z. Development of a Combined Device with High Vacuum and Pulsed Discharge Gas Chromatography and Its Application in Chemical Analysis of Gases from Rock Samples. *Rock Miner. Anal.* **2017**, *36*, 222−230.

(14) Cao, C.; Zhang, M.; Li, L.; Wang, Y.; Li, Z.; Du, L.; Holland, G.; Zhou, Z. Tracing the sources and evolution processes of shale gas by coupling stable (C, H) and noble gas isotopic compositions: Cases from Weiyuan and Changning in Sichuan Basin, China. *J. Nat. Gas Sci. Eng.* **2020**, *78*, No. 103304.

(15) Li, Z.; Wang, X.; Li, L.; Zhang, M.; Tao, M.; Xing, L.; Cao, C.; Xia, Y. Development of new method of $\delta^{13}C$ measurement for trace hydrocarbons in natural gas using solid phase micro-extraction coupled to gas chromatography isotope ratio mass spectrometry. *J. Chromatogr. A* **2014**, *1372*, 228−235.

(16) Cao, C.; Zhang, M.; Tang, Q.; Yang, Y.; Lv, Z.; Zhang, T.; Chen, C.; Yang, H.; Li, L. Noble gas isotopic variations and geological implication of Longmaxi shale gas in Sichuan Basin, China. *Mar. Pet. Geol.* **2018**, *89*, 38−46.

(17) Zhang, W.; Li, Y.; Zhao, F.; Han, W.; Li, Y.; Wang, Y.; Holland, G.; Zhou, Z. Using noble gases to trace groundwater evolution and assess helium accumulation in Weihe Basin, central China. *Geochim. Cosmochim. Acta* **2019**, *251*, 229−246.

(18) Zhang, T.; Zhang, M.; Bai, B.; Wang, X.; Li, L. Origin and accumulation of carbon dioxide in the Huanghua depression, Bohai Bay basin, China. *AAPG Bull.* **2008**, *92*, 341−358.

(19) Zhang, M.; Tang, Q.; Hu, P.; Ye, X.; Cong, Y. Noble gas isotopic constraints on the origin and evolution of the Jinchuan NieCue(PGE) sulfide ore-bearing ultramafic intrusion, West. China. *Chem. Geol.* **2013**, *339*, 301−312.

(20) Zhang, M.; Guo, Z.; Sano, Y.; Zhang, L.; Sun, Y.; Cheng, Z.; Yang, T. Magma-derived CO_2 emissions in the Tengchong volcanic field, SE Tibet: Implications for deep carbon cycle at intra-continent subduction zone. *J. Asian Earth Sci.* **2016**, *127*, 76−90.

(21) Xu, S.; Zheng, G.; Nakai, S.; Wakita, H.; Wang, X.; Guo, Z. Hydrothermal He and CO_2 at Wudalianchi intra-plate volcano, NE china. *J. Asian Earth Sci.* **2013**, *62*, 526−530.

(22) Thrasher, J.; Fleet, A. J. Predicting the Risk of Carbon Dioxide Pollution in Petroleum Reservoirs. In *Organic Geochemistry: Developments and Applications to Energy, Climate, Environment and Human History*; Grimalt, J. O.; Dorronsoro, C., Eds.; Proceedings of the 17th

International Meeting on Organic Geochemistry, San Sebastian, Spain, 1995; pp 1086−1088.
(23) Sano, Y.; Marty, B.; Burnard, P. Noble Gases in the Atmosphere. In *The Noble Gases as Geochemical Tracers*; Burnard, P., Ed.; Springer: Berlin, Heidelberg, 2013; pp 17−31.
(24) Mamyrin, B. A.; Anufriev, G. S.; Kamenskii, I. L.; Tolstikhin, I. N. Determination of the isotopic composition of atmospheric Helium. *Geochem. Int.* **1970**, *7*, 498−505.
(25) Sano, Y.; Wakita, H. Geographical distribution of $^3He/^4He$ ratios in Japan: Implications for arc tectonics and incipient magmatism. *J. Geophys. Res.: Solid Earth* **1985**, *90*, 8729−8741.
(26) Bottomley, D. J.; Ross, J. D.; Clarke, W. B. Helium and Neon isotope geochemistry of some ground waters from the Canadian Precambrian Shield. *Geochim. Cosmochim. Acta* **1984**, *48*, 1973−1985.
(27) Ballentine, C. J.; Bernard, M.; Sherwood, L. B.; Martin, C. Neon isotopes constrain convection and volatile origin in the Earth's mantle. *Nature* **2005**, *433*, 33−38.
(28) Sarda, P.; Staudacher, T.; Allègre, C. J. Neon isotopes in submarine basalts. *Earth Planet. Sci. Lett.* **1988**, *91*, 73−88.
(29) Kennedy, B. M.; Hiyagon, H.; Reynolds, J. H. Crustal neon: a striking uniformity. *Earth Planet. Sci. Lett.* **1990**, *98*, 277−286.
(30) Zhou, Z.; Ballentine, C. J.; Kipfer, R.; Schoell, M.; Thibodeaux, S. Noble gas tracing of groundwater/coalbed methane interaction in the San Juan Basin USA. *Geochim. Cosmochim. Acta* **2005**, *69*, 5413−5428.
(31) Mark, D. F.; Stuart, F. M.; de Podesta, M. New high-precision measurements of the isotopic composition of atmospheric argon. *Geochim. Cosmochim. Acta* **2011**, *75*, 7494−7501.
(32) Battani, A.; Sarda, P.; Prinzhofer, A. Basin scale natural gas source, migration and trapping traced by noble gases and major elements: the Pakistan Indus basin. *Earth Planet. Sci. Lett.* **2000**, *181*, 229−249.
(33) Ballentine, C. J.; Burgess, R.; Marty, B. Tracing fluid origin, transport and interaction in the crust. *Rev. Mineral. Geochem.* **2002**, *47*, 539−614.
(34) Graham, D. W. Noble Gas Isotope Geochemistry of Mid-ocean Ridge and Ocean Island Basalts: Characterization of Mantle Source Reservoirs. In *Noble Gases in Geochemistry and Cosmochemistry*; Porcelli, D.; Ballentine, C. J.; Weiler, R., Eds.; Reviews in Mineralogy and Geochemistry; Mineralogical Society of America: Washington, DC, 2002; pp 247−319.
(35) Andrews, J. N. The isotopic composition of radiogenic helium and its use to study groundwater movement in confined aquifers. *Chem. Geol.* **1985**, *49*, 339−351.
(36) Giggenbach, W. F.; Matsuo, S. Evaluation of results from Second and Third IAVCEI Field Workshops on Volcanic Gases, Mt Usu, Japan, and White Island, New Zealand. *Appl. Geochem.* **1991**, *6*, 125−141.
(37) Giggenbach, W. F.; Glover, R. B. Tectonic regime and major processes governing the chemistry of water and gas discharges from the rotorua geothermal field, New Zealand. *Geothermics* **1992**, *21*, 121−140.
(38) Fischer, T. P.; Giggenbach, W. F.; Sano, Y.; Williams, S. N. Fluxes and sources of volatiles discharged from Kudryavy, a subduction zone volcano, Kurile Islands. *Earth Planet. Sci. Lett.* **1998**, *160*, 81−96.
(39) Blomgren, V. J.; Crossey, L. J.; Karlstrom, K. E.; Fischer, T. P.; Darrah, T. H. Hot spring hydrochemistry of the Rio Grande rift in northern New Mexico reveals a distal geochemical connection between Valles Caldera and Ojo Caliente. *J. Volcanol. Geotherm. Res.* **2019**, *387*, No. 106663.
(40) Giggenbach, W. F. In *The Composition of Gases in Geothermal and Volcanic Systems as a Function of Tectonic Setting*, Proceedings of International Symposium on Water Rock Interaction, Roterdam, 1992; pp 873−878.
(41) Du, J.; Li, S.; Liu, L.; Ren, J.; Zhao, Y.; Sun, R.; Heshun, D. Geochemistry of gases from Wudalianchi volcanic district northeastern China. *Geochimica* **1999**, *28*, 171−176.
(42) Shangguan, Z.; Bai, C.; Sun, M. Mantle-derived magmatic gas releasing features at the Rehai area, Tengchong county, Yunnan Province, China. *Sci. China, Ser. D: Earth Sci.* **2000**, *43*, 132−140.
(43) Hoke, L.; Lamb, S.; Hilton, D. R.; Poreda, R. J. Southern limit of mantle-derived geothermal helium emissions in Tibet: implications for lithospheric structure. *Earth Planet. Sci. Lett.* **2000**, *180*, 297−308.
(44) Marty, B.; O'Nions, R. K.; Oxburgh, E. R.; Martel, D.; Lombardi, S. Helium isotopes in Alpine regions. *Tectonophysics* **1992**, *206*, 71−78.
(45) Wang, Q. *Crust-Mantle Electrical Structure and Dynamics of Xiaojinhe-Qinghe Tectonic Belt in the Central Sichuan-Yunnan Block*; Chengdu University of Technology, 2020; pp 38−56.
(46) Zhao, C.; Ran, H.; Wang, Y. Present-day mantle-derived helium release in the Tengchong volcanic field, Southwest China: Implications for tectonics and magmatism. *Acta Pet. Sin.* **2012**, *28*, 1189−1204.
(47) Shangguan, Z.; Zhao, C.; Gao, L. Carbon isotopic compositions of the methane derived from magma at the active volcanic regions in China. *Acta Pet. Sin.* **2006**, *22*, 1458−1464.
(48) Dai, J.; Yang, S.; Chen, H.; Shen, X. Geochemistry and occurrence of inorganic gas accumulations in Chinese sedimentary basins. *Org. Geochem.* **2005**, *36*, 1664−1688.
(49) Bergfeld, D.; Goff, F.; Janik, C. J. Carbon isotope systematics and CO_2 sources in the Geysers-Clear Lake region, northern California, USA. *Geothermics* **2001**, *30*, 303−331.
(50) Craig, H. The geochemistry of the stable carbon isotopes. *Geochim. Cosmochim. Acta* **1953**, *3*, 53−92.
(51) Xu, S.; Zheng, G.; Wang, X.; Wang, H.; Nakai, S.; Wakita, H. Helium and carbon isotope variations in Liaodong Peninsula, NE China. *J. Asian Earth Sci.* **2014**, *90*, 149−156.
(52) Marty, B.; Jambon, A. $C/^3He$ in volatile fluxes from the solid Earth: implications for carbon geodynamics. *Earth Planet. Sci. Lett.* **1987**, *83*, 16−26.
(53) Ballentine, C. J.; Burnard, P. Production of noble gases in the continental crust. *Rev. Mineral. Geochem.* **2002**, *47*, 481−538.
(54) Tao, H.; Wang, Q.; Yang, X.; Jiang, L. Provenance and tectonic setting of late Carboniferous clastic rocks in west Junggar, Xinjiang, China: a case from the Hala-alat Mountains. *J. Asian Earth Sci.* **2013**, *64*, 210−222.
(55) Xu, S.; Zheng, G.; Zheng, J.; Zhou, S.; Shi, P. Mantle-derived helium in foreland basins in Xinjiang, Northwest China. *Tectonophysics* **2017**, *694*, 319−331.
(56) Dubacq, B.; Bickle, M. J.; Evans, K. A. An activity model for phase equilibria in the H_2O-CO_2-NaCl system. *Geochim. Cosmochim. Acta* **2013**, *110*, 229−252.
(57) Gilfillan, S. M. V.; Lollar, B. S.; Holland, G.; Blagburn, D.; Stevens, S.; Schoell, M.; Cassidy, M.; Ding, Z.; Zhou, Z.; Lacrampe-Couloume, G.; Ballentine, C. J. Solubility trapping in formation water as dominant CO_2 sink in natural gas fields. *Nature* **2009**, *458*, 614−618.
(58) Clark, I. D.; Fritz, P. *Environmental Isotopes in Hydrology*; Lewis Publishers: New York, 1997; pp 55−61.
(59) Zhang, W.; Du, J.; Zhou, X.; Wang, F. Mantle volatiles in spring gases in the Basin and Range Province on the west of Beijing, China: Constraints from helium and carbon isotopes. *J. Volcanol. Geotherm. Res.* **2016**, *309*, 45−52.
(60) Sano, Y.; Marty, B. Origin of carbon in fumarolic gas from island arcs. *Chem. Geol.* **1995**, *119*, 265−274.
(61) Zhang, M.; Guo, Z.; Xu, S.; Barry, P. H.; Sano, Y.; Zhang, L.; Halldórsson, S. A.; Chen, A.; Cheng, Z.; Liu, C.; Li, S.; Lang, Y.; Zheng, G.; Li, Z.; Li, L.; Li, Y. Linking deeply-sourced volatile emissions to plateau growth dynamics in southeastern Tibetan Plateau. *Nat. Commun.* **2021**, *12*, No. 4157.
(62) Schoell, M. Multiple origins of methane in the Earth. *Chem. Geol.* **1988**, *71*, 1−10.
(63) Des Marais, D. J.; Donchin, J. H.; Nehring, M. L.; Truesdell, A. H. Molecular carbon isotopic evidence for the origin of geothermal hydrocarbons. *Nature* **1981**, *292*, 826−828.

https://doi.org/10.1021/acsomega.1c04533
ACS Omega 2021, 6, 30674−30685

(64) Poreda, R. J.; Craig, H.; Arnorsson, S.; Welhan, J. A. Helium isotopes in Icelandic geothermal systems: I. ^{3}He, gas chemistry, and ^{13}C relations. *Geochim. Cosmochim. Acta* **1992**, *56*, 4221−4228.
(65) McCollom, T. M.; Seewald, J. S. A reassessment of the potential for reduction of dissolved CO_2 to hydrocarbons during serpentinization of olivine. *Geochim. Cosmochim. Acta* **2001**, *65*, 3769−3778.
(66) Wen, H.; Sano, Y.; Takahata, N.; Tomonaga, Y.; Ishida, A.; Tanaka, K.; Kagoshima, T.; Shirai, K.; Ishibashi, J.; Yokose, H.; Tsunogai, U.; Yang, T. Helium and methane sources and fluxes of shallow submarine hydrothermal plumes near the Tokara Islands, Southern Japan. *Sci. Rep.* **2016**, *6*, No. 34126.
(67) Kulongoski, J. T.; Hilton, D. R.; Barry, P. H.; Esser, B. K.; Hillegonds, D.; Belitz, K. Volatile fluxes through the Big Bend section of the San Andreas Fault, California: helium and carbon-dioxide systematics. *Chem. Geol.* **2013**, *339*, 92−102.
(68) Kennedy, B. M.; Kharaka, Y. K.; Evans, W. C.; Ellwood, A.; DePaolo, D. J.; Thordsen, J.; Ambats, G.; Mariner, R. H. Mantle fluids in the San Andreas fault system, California. *Science* **1997**, *278*, 1278−1281.
(69) Zhang, M.; Guo, Z.; Sano, Y.; Zhang, L.; Sun, Y.; Cheng, Z.; Yang, T. Magma-derived CO_2 emissions in the Tengchong volcanic field, SE Tibet: Implications for deep carbon cycle at intra-continent subduction zone. *J. Asian Earth Sci.* **2016**, *127*, 76−90.
(70) Jiang, W.; Zhang, J.; Tian, T.; Wang, X. Crustal structure of Chuan-Dian region derived from gravity data and its tectonic implications. *Phys. Earth Planet. Inter.* **2012**, *212*−*213*, 76−87.
(71) Dong, X.; Yang, D.; Niu, F. Passive adjoint tomography of the crustal and upper mantle beneath eastern Tibet with a W2 norm misfit function. *Geophys. Res. Lett.* **2019**, *46*, 12986−12995.
(72) Bao, X.; Sun, X.; Xu, M.; Eaton, D. W.; Song, X.; Wang, L.; Ding, Z.; Mi, N.; Li, H.; Yu, D.; Huang, Z.; Wang, P. Two crustal low-velocity channels beneath SE Tibet revealed by joint inversion of Rayleigh wave dispersion and receiver functions. *Earth Planet. Sci. Lett.* **2015**, *415*, 16−24.
(73) Burchfiel, B. C.; Chen, Z. *Tectonics of the Southeastern Tibetan Plateau and its Adjacent Foreland*; The Geological Society of America: Memior 210, 2012; pp 37−52.
(74) Wei, F.; Xu, J.; Shangguan, Z.; Pan, B.; Yu, H.; Wei, W.; Bai, X.; Chen, Z. Helium and carbon isotopes in the hot springs of Changbaishan Volcano, northeastern China: A material connection between Changbaishan Volcano and the west Pacific plate? *J. Volcanol. Geotherm. Res.* **2016**, *327*, 398−406.
(75) Burnard, P.; Bourlange, S.; Henry, P.; Geli, L.; Tryon, M. D.; Natal'in, B.; Sengör, A. M. C.; Özeren, M. S.; Çagatay, M. N. Constraints on fluid origins and migration velocities along the Marmara Main Fault (Sea of Marmara, Turkey) using helium isotopes. *Earth Planet. Sci. Lett.* **2012**, *341*−*344*, 68−78.
(76) Klemperer, S. L.; Kennedy, B. M.; Sastry, S. R.; Makovsky, Y.; Harinarayana, T.; Leech, M. L. Mantle fluids in the Karakoram fault: helium isotope evidence. *Earth Planet. Sci. Lett.* **2013**, *366*, 59−70.
(77) Tanikawa, W.; Sakaguchi, M.; Tadai, O.; Hirose, T. Influence of fault slip rate on shear-induced permeability. *J. Geophys. Res.* **2010**, *115*, No. B07412.
(78) Wang, Y.; Liu, Y.; Zhao, C.; Li, Q.; Zhou, Y.; Ran, H. Helium and carbon isotopic signatures of thermal spring gases in southeast Yunnan, China. *J. Volcanol. Geotherm. Res.* **2020**, *402*, No. 106995.
(79) Wang, Y.; Wang, E.; Shen, Z.; Wang, M.; Gan, W.; Qiao, X.; Meng, G.; Li, T.; Tao, W.; Yang, Y.; Cheng, J.; Li, P. GPS-constrained inversion of present-day slip rates along major faults of the Sichuan-Yunnan region, China. *Sci. China, Ser. D: Earth Sci.* **2008**, *51*, No. 1267.

https://doi.org/10.1021/acsomega.1c04533
ACS Omega 2021, 6, 30674−30685